CAMBRIDGE ACOUSTICAL ASSOCIATES

A DEVICE FOR MEASURING THE PROPERTIES OF ACOUSTIC MATERIALS AT LOW FREQUENCY UNDER PRESSURE

Prepared by:
John E. Cole, III and Kyle Martini

March 2, 1994

Final Report U-2211-390
Prepared under Contract N00014-93-C-0041 for:
Office of Naval Research
800 N. Quincy Street
Arlington, VA 22217-5660
Attn: Dr. Kam W. Ng

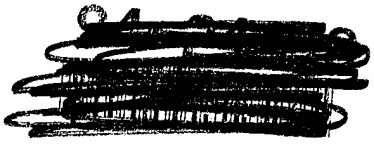

, SUITE 2500, MEDFORD, MA 02155

A DEVICE FOR MEASURING THE PROPERTIES OF ACOUSTIC MATERIALS AT LOW FREQUENCY UNDER PRESSURE

Prepared by:
John E. Cole, III
and
Kyle Martini

March 2, 1994

Final Report U-2211-390

Prepared under Contract N00014-93-C-0041 for:
Office of Naval Research
800 N. Quincy Street
Arlington, VA 22217-5660
Attn: Dr. Kam W. Ng

Cambridge Acoustical Associates, Inc.
200 Boston Avenue, Suite 2500
Medford, MA 02155-4243

TABLE OF CONTENTS

EXECUTIVE SUMMARY

Under the Attenuation Material Program of the Office of Naval Research, Cambridge Acoustical Associates has developed a laboratory device for characterizing acoustic materials at low frequencies (viz., below 2 kHz) and under hydrostatic pressure up to 500 psig. The device shown on Fig. 1 is a compact pressure chamber that accommodates 4 inch diameter material samples. Excitation is by means of a specially designed impedance head. A unique feature of this device is a water layer that couples the impedance head and the material sample. This permits realistic excitation of materials that deform under hydrostatic loading. The material sample is inertially backed by a steel mass. The design of the device is documented in Ref. 1.

Both the input impedance and vibration transmissibility across the inertially backed sample are measured with the device. These measurements are used in expressions derived from a plane-wave acoustic model (see Appendix) to determine direct and transfer impedances of the material itself.

Measurements have been made on water columns and on an air-rubber material sample to evaluate the performance of the device. The water column data are shown on Figs. 4. Vibration transmissibility measurements can be made throughout the design frequency range. Under conditions of low loading, electrical interference is present in the force gage measurements below approximately 400 Hz. Data from tests on the air-rubber material at 50 psig using two water layer thicknesses are given on Figs. 7. Using the plane wave analysis given in the Appendix, the two-port impedances that characterize the material itself are derived and presented in Figs. 8. These results show a strong absorption band between 600 and 700 Hz where the magnitude of the blocked impedance Z_{11} approaches that of water and the phase approaches that of a pure resistance.

Although further work is needed to improve the performance of the force gage, existing capabilities of the device permit measurements of vibration transmissibility over the full frequency bandwidth and of input impedance above approximately 400 Hz. The device is available for characterizing low frequency materials of interest and can be used to obtain comparison measurements with other low frequency test facilities.

I. INTRODUCTION

Development of materials for underwater acoustic applications requires measurement facilities for characterizing acoustic performance. Existing facilities are generally suitable for making measurements in the frequency range above 1 kHz. These include the pulse tubes located at NSWC/Annapolis and the anechoic tank located at NRL/Orlando.

Under the Attenuation Materials Program of the Office of Naval Research, capabilities for characterizing acoustical materials in the frequency range below 1 kHz are being developed and improved. As part of this effort, Cambridge Acoustical Associates has designed and developed a laboratory testing device for evaluating acoustical materials below 1 kHz at hydrostatic pressures up to 500 psig.

Several unique testing capabilities are designed into this device. Sufficient measurements are made on inertially-backed samples to obtain a two-port impedance representation of the material. A water layer coupling the excitation piston and the face of the material sample permits realistic loading of spatially inhomogeneous materials under hydrostatic pressure.

The design of the device is documented in Ref. 1. In this report the performance of the device is evaluated.

II. DESCRIPTION AND USAGE

A. Concept and Design

The device shown on Fig. 1 is designed to enable measurements of the two-port impedance matrix of an acoustical material, that is, direct and transfer impedances across the material faces. This requires pressure and velocity measurements on both faces of the sample. On the excitation side, the measurements are accomplished by an impedance head designed and developed for the device. The "transmitted" side of the material is backed by an inertial backing plate whose motion is measured by an accelerometer. The inertial backing is obtained by having a low impedance air space above the backing mass. Under this condition, the acceleration measurement is sufficient to determine the pressure acting on the "transmitted" side of the sample.

A unique feature of the device is a layer of water that couples the driver to the material face. This layer is introduced so that spatially inhomogeneous materials, whose surface may deform under hydrostatic pressure, can be realistically excited.

The chamber is a sealed tube having an internal diameter of 4 inches and designed to withstand an internal pressure of 500 psig. As indicated in Fig. 1, the bottom section contains the driver, the sample, and the intermediate water layer. Removal of the air-filled top section provides access for inserting the material sample. Pneumatic and hydraulic connections to both sections permit water filling and pneumatic pressurization. Electrical feed-throughs for the two accelerometers, force gage, and driver are mounted in the top and bottom blind flanges.

1. Pressure Chamber

The pressure chamber is fabricated from steel pipe having a wall thickness of 0.25 inch. The resulting stiffness of the chamber under hydrostatic pressurization is approximately five times the bulk modulus of water (i.e., $Eh/2a\rho c^2 = 5.2$, where E is elastic modulus, a is radius, h is thickness, and ρc^2 is the bulk modulus of water). Flanges are welded onto the ends of both chamber sections. The chamber is designed in accordance with ASME pressure vessel codes for working pressures up to 500 psig. Electrical feed-throughs for the accelerometers, force gage, and driver power supply are rated for more than 1000 psig.

O-rings seal the joints between chamber sections and also seal the liquid from the air at both the piston and the sample backing mass. A tight clearance (0.004")between the tube wall and both the drive piston and backing mass is maintained to minimize acoustic effects of the air-backed slot [1].

2. Impedance Head

Excitation of the material sample is by means of a piezoelectric driver containing a force gage. The tonpilz driver comprising 12 PZT-8 ring elements is indicated on Fig. 1. Head and tail masses are 1.5 inch thick aluminum and 4.5 inch thick steel, respectively.

The driver is designed to obtain a 1 micron displacement with a voltage not exceeding 500 volts. The electrical admittance increases with frequency below the driver resonance of 4,380 Hz.

The force gage consists of two PZT-8 rings located between the head mass and the driver piston. The measured sensitivity of this gage is -180.8 dB re: $V/\mu Pa$.

The drive piston is a 0.38 inch thick beryllium plate. Having both high modulus and low weight, beryllium is used to maintain a stiff piston surface over the test frequency range while minimizing the inertia above the force gage. The invacuo natural frequency of the piston excited through the force gage is 12 kHz.

Axial motion of the driver tail mass is isolated from the base of the test chamber using a spring.

3. Sample Installation Procedure

A design requirement of the test device is to minimize air content in the water layer. This is achieved through use of de-aerated water and by the filling and pressurization procedure.

Sample installation begins with the driver in place and the top section of the chamber removed. The distance from the top of the drive piston to the top of the bottom section is measured to determine the lower level of the water column. The sample and its attached backing mass are inserted into the test chamber at its desired location and locked into place using mechanical stops. The top section of the chamber is then bolted in place.

Filling begins with simultaneous evacuation of air from all sections of the test chamber and the fill line of the de-aerated water supply. Once the air is evacuated, the fill line and test section are isolated from the other sections by a shut-off valve, and de-aerated water is admitted under atmospheric pressure. Once water has filled the test section, the top and bottom sections are pressurized to atmospheric pressure.

The distance between the top of the backing plate and the top of the bottom section is measured to determine the length of the water column. This length is checked at the completion of the test by measuring the amount of water and re-measuring the location of the piston face.

The system is conditioned by pressurization to 500 psig for a period of 12 hours. A minimum of 20-40 psig is maintained in the system during testing.

B. Instrumentation And Cabling

1. Driver

A schematic diagram of the instrumentation electronics is given in Fig. 2. Excitation signals for the driver are generated by a Wavetek Model 185 signal generator capable of providing steady state tones and sinusoidal sweeps. This signal is amplified by a 100 watt audio amplifier.

Because of the low driver admittance at low frequency, a 20:1 turn transformer is used between the amplifier and driver to improve the impedance match. Furthermore, to avoid resonance excitation of the driver, a low pass filter designed to cut off above 2 kHz is used after the transformer.

The driver is excited through twisted pair conductors that connect via a three-pin feed-through in the chamber base plate. The third pin carries an isolated shield.

2. Sensors

Motion of the drive piston is measured by an accelerometer (Wilcoxon 736T, 100 mV/g) located on the top mass of the tonpilz driver. As indicated on Fig. 1, the force gage is located between the driver top mass and the beryllium piston. The accelerometer is eccentrically located on the top mass and balanced by an opposed "dummy" accelerometer. In the operating frequency range, the stiffness of the force gage and piston is sufficiently large to provide a unity transfer function between the driver top mass and the piston.

The accelerometer located in the center of the sample backing mass (Wilcoxon 768, 500 mV/g) senses the transfer motion of the material sample.

Signals from both accelerometers are fed through coaxial cables terminated by BNC connectors on the inside of the chamber. The pressure feed-throughs provide BNC connectors on the inside and outside of the chamber. External cables connect the accelerometers to their power supplies and charge amplifiers (Wilcoxon P702B).

The signal from the force gage is carried by coaxial cables to a BNC feed-through on the chamber base plate. Outside the chamber the force gage is connected to an impedance inverter (Wilcoxon CC7011) and power unit (Wilcoxon P704B) followed by a pre-amp (Wilcoxon AM-5).

C. Data Acquisition And Signal Processing

A sine chirp signal is used to excite the driver. Although random noise can be used, results are more stable under chirp excitation.

Signals from the two accelerometers and the force gauge are acquired using CAA's digital signal processing computer [2]. The three signals are digitized based on a Nyquist criterion for the operating bandwidth (typically 2.5 times above the maximum frequency of interest).

Two methods for forming transfer functions between the sensors are available. In the absence of noise, the transfer function can be obtained from the ratio of the two autospectra. Alternatively, the cross spectra of the two signals can be obtained and averaged over multiple excitation chirps. The transfer function is then obtained by normalizing the cross spectrum to the appropriate autospectra.

III. DATA ANALYSIS

Measurements of the input acoustic impedance and acceleration transmissibility across the material sample are made for each test. These measurements include the presence of the water coupling layer and the backing mass. Both the coupling layer and the backing mass are well characterized (e.g., known density, thickness, sound speed, etc.). Consequently, their effects can be removed from the measurements through use of an acoustic model of the test device.

The plane wave model shown on Fig. 3 includes the water coupling layer, an equivalent layer representing the test material, and the backing mass. The test material is described by a thickness, equivalent density, sound speed, and loss factor. A two-port characterization of the material layer is given by

$$\begin{bmatrix} p_1 \\ p_2 \end{bmatrix} = \begin{bmatrix} Z_{11} Z_{12} \\ Z_{21} Z_{22} \end{bmatrix} \begin{bmatrix} \dot{w}_1 \\ \dot{w}_2 \end{bmatrix} \qquad (1)$$

where the subscripts 1 and 2 refer respectively to the front and back surfaces of the sample. For linear materials, this impedance matrix is reciprocal and the diagonal and off-diagonal terms are equal and of opposite sign.

In terms of the measured quantities, the two-port representation is:

$$\begin{bmatrix} p_o \\ p_2 \end{bmatrix} = \begin{bmatrix} \zeta_{11} \zeta_{12} \\ \zeta_{21} \zeta_{22} \end{bmatrix} \begin{bmatrix} \dot{w}_o \\ \dot{w}_2 \end{bmatrix} \tag{2}$$

where the ζ_{ij} include the effects of the coupling layer and the backing mass. The relationships between the ζ_{ij}'s, the Z_{ij}'s, and the measurements are given in the Appendix. In the limit of an acoustically thin liquid layer and a sufficiently "soft" material layer, the resulting expressions for the material impedances in terms of the measured quantities are given by

$$Z_{11} \cong -\left[\frac{Z_o + Z_M (\dot{w}_2/\dot{w}_0)^2 - Z_{M_w}}{(1 + Z_M/Z_{K_w})(\dot{w}_2/\dot{w}_0)^2 - 1 + Z_o/Z_{K_w}} \right] \tag{3a}$$

$$Z_{12} \cong \frac{(Z_o + Z_M - Z_{M_w})\dot{w}_2/\dot{w}_0}{[(1 + Z_M/Z_{K_w})(\dot{w}_2/\dot{w}_0)^2 - 1 + Z_o/Z_{K_w}]} \tag{3b}$$

where $Z_o \equiv p_o/\dot{w}_o$ is the input impedance, Z_M is the inertial impedance of the backing mass, Z_{M_w} is the inertial (viz., free) impedance of the water column, and Z_{K_w} is the stiffness (viz., blocked) impedance of the water column.

IV. RESULTS AND DISCUSSION

A. Water Columns

1. Measurements

Measurements made on water columns of different height are used to evaluate the performance of the testing device. Because of the low damping of this "material", these tests provide not only a calibration of the device but also relatively harsh loading conditions.

Shown on Fig. 4a is the measured vibration transmissibility ($\dot{w}_2/\dot{w}_o$) of 5.1, 6.1, and 7.1 inch water columns backed by a 0.5 inch steel plate. Both magnitude and relative phase of the data are plotted in the frequency range between 250 and 1500 Hz.

The dominant feature of the vibration transmissibility is the antiresonance peak and associated phase change of the inertially-backed water columns. This frequency increases as the column height decreases. Both top and bottom accelerometers are in phase at low frequency and out-of-phase above the antiresonance frequency. These measured transmissibilities are characteristic of a single degree-of-freedom system consisting of a mass-backed elastic column.

Several features of the water column transmissibilities are noted. The low frequency data are somewhat irregular owing to low driver amplitude within the broadband excitation used for these data. Measurements for a 3.1 inch water column using an excitation bandwidth of 50-500 Hz are shown on Fig. 4b along with broader bandwidth data. Improvement at low frequency is evident.

The input impedance measurements shown on Fig. 4c have similar characteristics to the measured transmissibilities. In this case the antiresonance peak corresponds to a high input impedance. The magnitude of the impedance is normalized to the characteristic impedance of water based on the effective sound speed in the chamber (see following section).

The width of the antiresonance peak is a measure of the system damping. Effective loss factors calculated from the data of Fig. 4c are in the range of η=0.03. The most likely source of system damping having this magnitude is shear deformation of the rubber O-rings that seal the drive piston and the sample top mass.

The relative phase measurements deviate from their anticipated inertial value of -90° at frequencies below approximately 450 Hz. This deviation is due to contamination of the force gage signal. The source of contamination is interference (i.e., cross-coupling) with the high-voltage excitation signal to the driver, and the extent of the contamination depends on the dynamic characteristics of the sample being tested. Greater dynamic loads at low frequencies than obtained with the primarily inertial water columns at low frequencies push the useful range of the force gage to lower frequencies. Further modifications in shielding and/or grounding are needed to improve the force gage performance.

To some extent, all water column data display a "kink" near 1 kHz. The reason for this feature is the fundamental axisymmetric axial (i.e., accordion) mode of the test chamber (i.e., pipe section and flanges) which occurs near 1 kHz. Through Poisson coupling, this mode is excited by the acoustic pressure in the water layer. In the immediate vicinity of the accordion mode resonance frequency, the compliance of the pipe wall changes rapidly [3] which modifies the effective sound speed in the water from the Korteweg-Lamb value given below (Eq. 4).

The occurrence of this lightly damped vibrational mode near the upper end of the nominal operating frequency range has little impact on the performance of the device. Any effect on the measurements is localized to the immediate vicinity of 1 kHz. The use of short water columns minimizes coupling into the accordion mode. Should measurements be required near 1 kHz, an axial dynamic vibration absorber tuned to the chamber's resonance frequency should be effective in shifting the resonance frequency away from the test range of interest.

2. Predictions

Predictions of the water column tests results are obtained using both plane-wave and finite element models. The axisymmetric finite element model includes the elasticity of the drive piston as well as the associated non-planar components of the excitation and response. Both models assume rigid chamber walls and account for the wall compliance through the effective sound speed given by the Korteweg-Lamb result [4]

$$c_e = \frac{c_w}{\sqrt{1 + 2\alpha\rho c_w^2 / Eh}} \qquad (4)$$

For the chamber material and dimensions, the effective sound speed is 0.924 that of water.

Measurements of the 7.1" water column are compared with the predictive models on Figs. 5a and 5b. The antiresonance frequency predicted from the plane wave model is 5.6% higher than that measured, while the finite element prediction is consistent with the measurements. Elastic deformation of the piston is therefore responsible for most of the additional compliance not accounted for by the chamber wall elasticity. The relatively high antiresonance frequencies of the water column tests (i.e., above 1 kHz) tend to enhance the added compliance of the piston

by operating closer to its fundamental elastic resonance. Piston compliance is not expected to be as significant in material tests made in the frequency range below 1 kHz.

B. Air-Rubber Sample

Measurements have been made on an air-rubber material that was developed for a low-frequency absorber [5]. Dimensions and geometry are shown on Fig. 6 for the rubber tile. Measurements of the dynamic material properties indicate a peak loss factor of 1.0 occurring at 20°C and approximately 30 Hz. Finite element calculations and bench top measurements indicate the static stiffness of the tile to be in the range of 15,000 psi/in. Used in the plane wave model, these parameters obtain an antiresonance frequency near 600 Hz.

Measurements are made on the sample with several water layer thicknesses and hydrostatic pressures. Shown on Figs. 7a and 7b are respectively the vibration transmissibilities and input impedance measurements with 2.5 and 4.5 inch water layers at a hydrostatic pressure of 50 psig. Data below approximately 400 Hz begin to contain effects of the force gage signal contamination. The antiresonance peaks of both tests are located near 700 Hz.

Measurements for both water layer thicknesses are used in Eqs. 3 to derive the two-port impedances of the material layer. The measurements of Figs. 7 are smoothed to remove some of the small scale fluctuations. The magnitude and phase of the resulting direct and transfer material impedances (i.e., Z_{11} and Z_{12}) are given in Figs. 8a and 8b. Measurements from both water layer tests yield similar results. The magnitude of the normalized blocked impedance Z_{11} peaks at a value of approximately 0.8, and near this peak the phase is close to zero. Within this region the material behaves as an effective acoustic absorber. Well away from the frequency range of the peak, the phase indicates primarily spring-like behavior. The peak of the transfer impedance Z_{12} is comparable in magnitude to that of Z_{11}, and in this frequency range, the transfer velocity and force are out-of-phase.

The differences between the derived impedances shown in Figs. 8 primarily reflect measurement uncertainties of the device. Estimates of uncertainty associated with the measurements needed to derive the two-port material impedances

are the following: acceleration transmissibility (±3%); input impedance (±10%); water depth (±0.1 inch); hydrostatic pressure (±5 psi).

V. CONCLUSIONS AND RECOMMENDATIONS

Evaluations performed on the laboratory test device have demonstrated the following capabilities:

(a) Hydrostatic pressurization up to 500 psig;
(b) Vibration transmissibility measurements from 50-1000 Hz;
(c) Input impedance measurements from approximately 400 to 1000 Hz.

Over the operating range of the device, the measurements permit characterization of the acoustic response of materials as a two-port impedance matrix.

The following recommendations for further development and utilization of this device are made:

(1) Improvement in the performance of the force gage at low frequency is needed to extend the full capability of the test device. Since electrical interference appears to be contaminating low frequency signals from the force gage, improved electrical shielding and grounding should effectively increase the performance of this sensor.
(2) The effect of the drive piston compliance on the device performance needs to be quantified. Means to do this include (a) using an improved force gage to better assess the compliance of the chamber walls and (b) measuring the response of known materials at lower frequencies.
(3) The device should be used to measure materials of interest that have been evaluated in other test facilities (e.g., pulse tubes, anechoic tanks). Comparison of test results would permit existing material test capabilities at low frequency to be assessed.

REFERENCES

1 J.E. Cole, III and K. Martini, Low Frequency Material Testing Device Design, (CAA Report U-2152-390, prepared for the Office of Naval Research, 20 October 1993).

2 SIGNAL, (Engineering Design, Belmont, MA 1990).

3 J.E. Cole, III, "Shell Response Characteristics to Excitation by Axial Loads", (CAA Report U-1796-371, prepared for AT&T Bell Laboratories, Feb. 1990).

4 M.C. Junger and D. Feit, Sound, Structures and Their Interaction, (2nd Ed., MIT Press, Cambridge, MA, 1986) pp. 41-43.

5 J. Cole, "Development of the CAA SSL Wedge", (CAA TM/U-1664-358.2, prepared under contract N00167-86-C-0028 for David W. Taylor Naval Ship R&D Center, 28 Nov. 1988).

APPENDIX:
TWO-PORT MATERIAL IMPEDANCES DERIVED FROM DEVICE MEASUREMENTS

A. ACOUSTIC LAYER MODEL

The model of the testing system (Fig. 1) shows the material layer backed by a mass and coupled to the driver by a fluid column. The material sample is assumed to be characterized as a two-port linear system,

$$\begin{bmatrix} p_1 \\ p_2 \end{bmatrix} = \begin{bmatrix} Z_{11} Z_{12} \\ Z_{21} Z_{22} \end{bmatrix} \begin{bmatrix} \dot{w}_1 \\ \dot{w}_2 \end{bmatrix} \qquad (A-1)$$

where the subscripts 1 and 2 refer respectively to the front and back surfaces of the sample. The four impedances completely characterize the material sample and permit any response function to be calculated (e.g., transmission, reflection, absorption).

Within the material layer, pressure and normal velocity are expressed in terms of waves propagating at the effective material sound speed,

$$p(x) = Ae^{ik_L x} + Be^{-ik_L x}$$

$$\dot{w}(x) = \frac{1}{\rho_L c_L}\left[Ae^{ik_L x} - Be^{-ik_L x}\right] \qquad (A-2)$$

where A and B, respectively, are the amplitudes of the forward and backward propagating waves. The two boundary conditions specified to determine the amplitudes are

$$p(x=0) = p_1$$

$$\left.\frac{p}{\dot{w}}\right|_{x=H} = Z_M \qquad (A-3)$$

where $Z_M = -i\omega\rho_M H_M$ is the inertial impedance of the backing mass of density ρ_M and thickness H_M.

The solution to Eqs. A-2 and A-3 for pressure and velocity is

$$\frac{p(x)}{p_1} = \frac{\hat{Z}_M \cos k_L(H_L - x) - i\sin k_L(H_L - x)}{\hat{Z}_M \cos k_L H_L - i\sin k_L H_L} \qquad (A-4a)$$

$$\frac{\rho_L c_L \dot{w}(x)}{p_1} = \frac{\cos k_L(H_L - x) - i\hat{Z}_M \sin k_L(H_L - x)}{\hat{Z}_M \cos k_L H_L - i\sin k_L H_L} \qquad (A-4b)$$

where $\hat{Z}_M \equiv Z_M/\rho_L c_L$. From this solution the impedance looking into the sample is calculated:

$$Z_L = \frac{p(o)}{\dot{w}(o)} = \frac{p_1}{\dot{w}_1} = \rho_L c_L \left[\frac{\hat{Z}_M \cos k_L H_L - i \sin k_L H_L}{\cos k_L H_L - i \hat{Z}_M \sin k_L H_L} \right] \qquad (A\text{-}5a)$$

The low frequency limit of this impedance (i.e., $k_L H_L \to 0$) is given by

$$Z_L = \frac{Z_M - i\omega\rho_L H_L}{1 - i Z_M \omega H_L/\rho_L c_L} = \frac{-i\omega(\rho_m H_M + \rho_L H_L)}{1 - (\omega/\omega_o)^2} \qquad (A\text{-}5b)$$

where

$$\omega_o^2 = \frac{\rho_L c_L^2/H_L}{\rho_M H_M} \equiv \frac{K_L}{M_M}$$

is the resonance frequency of the backing plate mass (M_M) on the layer stiffness (K_L). In the frequency range well below ω_o, impedance Z_L represents the inertia of the layer and its backing mass. Frequency ω_o is an antiresonance of the mass-backed layer. Limits obtained for infinite (viz. blocked) and zero backing impedances are respectively

$$Z_L\big|_{Z_M \to 0} = -i\rho_L c_L \tan k_L H_L; \qquad (A\text{-}5c)$$

$$Z_L\big|_{Z_M \to \infty} = i\rho_L c_L \cot k_L H_L \qquad (A\text{-}5d)$$

The equations of the two-port model given in Eq. A-1 can be written

$$\frac{p_1}{\dot{w}_1} = Z_{11} + Z_{12}\frac{\dot{w}_2}{\dot{w}_1} \qquad (A\text{-}6a)$$

$$\frac{p_2}{\dot{w}_2} = Z_{21}\frac{\dot{w}_1}{\dot{w}_2} + Z_{22} \qquad (A\text{-}6b)$$

The impedances on both sides of the layer as well as the velocity ratio across the layer are calculated from Eqs. A-4 and A-5a

$$\frac{p_1}{\dot{w}_1} = Z_L \qquad (A\text{-}7a)$$

$$\frac{P_2}{\dot{w}_2} = Z_M \qquad (A\text{-}7b)$$

$$\frac{\dot{w}_1}{\dot{w}_2} = \cos k_L H_L - i\hat{Z}_M \sin k_L H_L \qquad (A\text{-}7c)$$

As seen from Eqs. A-6, the two diagonal entries of the impedance matrix are the blocked impedances which, except for a sign reversal, are given by Eq. A-5d

$$Z_{11} = i\rho_L c_L \cot k_L H_L$$

$$Z_{22} = -Z_{11} \qquad (A-8)$$

The blocked transfer impedances (Z_{12} and Z_{21}) in Eq. A-6 are obtained by substituting Eqs. A-7 and A-8 into Eq. A-6, the result being

$$Z_{12} = -Z_{21} = -i\rho_L c_L \csc k_L H_L \qquad (A-9)$$

B. FLUID COUPLING LAYER

The two-port representation of the acoustic layer given in Eqs. A-7 through A-9 is expressed in terms of the velocities and pressures at the forward and back surfaces of the material layer. In the testing device, measurements are made at the back surface and at the drive end of the fluid coupling layer. Consequently, forward surface quantities are expressed in terms of those measured at the face of the driver.

The presence of the fluid is modeled by including a fluid layer between the driver and the forward face of the material layer. This model is identical to that assumed for the mass-backed layer, and a similar solution results. Although both pressure and velocity are measured in the testing device, we assume a velocity boundary condition at the drive

$$\dot{w}(x=0) = \dot{w}_o \qquad (A-10)$$

The impedance terminating the fluid layer is that looking into the layer (i.e., Z_L, Eq. A-5a). The solutions for pressure and velocity anywhere in the fluid layer are given by

$$\dot{w}(x) = \dot{w}_o \frac{\cos k_w(H_w - x) - i\tilde{Z}_L \sin k_w(H_w - x)}{\cos k_w H_w - i\tilde{Z}_L \sin k_w H_w} \qquad (A-11a)$$

$$p(x) = \rho_w c_w \dot{w}_o \frac{\tilde{Z}_L \cos k_w(H_w - x) - i\sin k_w(H_w - x)}{\cos k_w H_w - i\tilde{Z}_L \sin k_w H_w} \qquad (A-11b)$$

where $\tilde{Z} \equiv Z_L/\rho_w c_w$ is the input impedance of the layer normalized to the characteristic impedance of the fluid. From these results, we calculate the pressure and velocity ratios which

relate the quantities at the front surface of the layer to the corresponding quantities measured at the driver

$$\frac{\dot{w}_1}{\dot{w}_o} \equiv \frac{\dot{w}(H_w)}{\dot{w}(o)} = \frac{1}{\cos k_w H_w - i\tilde{Z}_L \sin k_w H_w} \qquad (A-12a)$$

$$\frac{p_1}{p_o} = \frac{p(H_w)}{p(o)} = \frac{\tilde{Z}_L}{\tilde{Z}_L \cos k_w H_w - i \sin k_w H_w} \qquad (A-12b)$$

Because the fluid layer is short in terms of acoustic wavelengths (i.e., $(k_w H_w)^2 \ll 1$), these expressions simplify to the following:

$$\frac{\dot{w}_1}{\dot{w}_o} \cong \frac{1}{1 + Z_L / Z_{K_w}} \qquad (A-13a)$$

$$\frac{p_1}{p_o} \cong \frac{Z_L}{Z_L + Z_{M_w}} \qquad (A-13b)$$

where $Z_{K_w} = i\rho_w c_w^2 / \omega H_w$ is the stiffness impedance of the water column and $Z_{M_w} = -i\omega\rho_w H_w$ is its mass impedance.

The two-port model of the entire system including the coupling fluid, material layer, and its backing mass is obtained by substituting Eqs. A-13 into Eq. A-1. This permits the relationship between pressure and velocity at the driver and those at the backside of the sample to be expressed as follows:

$$\begin{bmatrix} p_o \\ p_2 \end{bmatrix} = \begin{bmatrix} \zeta_{11} \zeta_{12} \\ \zeta_{21} \zeta_{22} \end{bmatrix} \begin{bmatrix} \dot{w}_o \\ \dot{w}_2 \end{bmatrix} \qquad (A-14)$$

The model impedances are given by

$$\zeta_{11} = \frac{Z_{11} + Z_{M_w}}{1 + Z_{11} / Z_{K_w}} \qquad (A-15a)$$

$$\zeta_{12} = Z_{12} \left[\frac{1 - Z_{M_w} / Z_{K_w}}{1 + Z_{11} / Z_{K_w}} \right] \qquad (A-15b)$$

$$\zeta_{21} = \frac{-Z_{12}}{1 + Z_{11} / Z_{K_w}} \qquad (A-15c)$$

$$\zeta_{22} = -\left[\frac{Z_{11} + (\rho_L c_L)^2 / Z_{K_w}}{1 + Z_{11} / Z_{K_w}} \right] \qquad (A-15d)$$

Equations A-14 and A-15 contain the two impedances of the two-port material layer model Z_{11} and Z_{12}. These impedances can be expressed in terms of the three measurements $p_o, \dot{w}_o, \dot{w}_2$ after using the mass law termination condition $p_2 = Z_M \dot{w}_2$.

To simplify the results we assume an acoustically thin fluid layer (i.e., $(k_w H_w)^2 \ll 1$)) and a "soft" layer relative to its backing mass (i.e., $(\rho_L c_L / \rho_w c_w)^2 Z_{M_w} / Z_M \ll 1$). The resulting expressions for the two-port layer impedances are

$$Z_{11} \cong -\left[\frac{Z_o + Z_M (\dot{w}_2/\dot{w}_0)^2 - Z_{M_w}}{(1 + Z_M/Z_{K_w})(\dot{w}_2/\dot{w}_0)^2 - 1 + Z_o/Z_{K_w}} \right] \qquad (A-16a)$$

$$Z_{12} \cong \frac{(Z_o + Z_M - Z_{M_w})\dot{w}_2/\dot{w}_0}{[(1 + Z_M/Z_{K_w})(\dot{w}_2/\dot{w}_0)^2 - 1 + Z_o/Z_{K_w}]} \qquad (A-16b)$$

where $Z_o \equiv p_o/\dot{w}_o$.

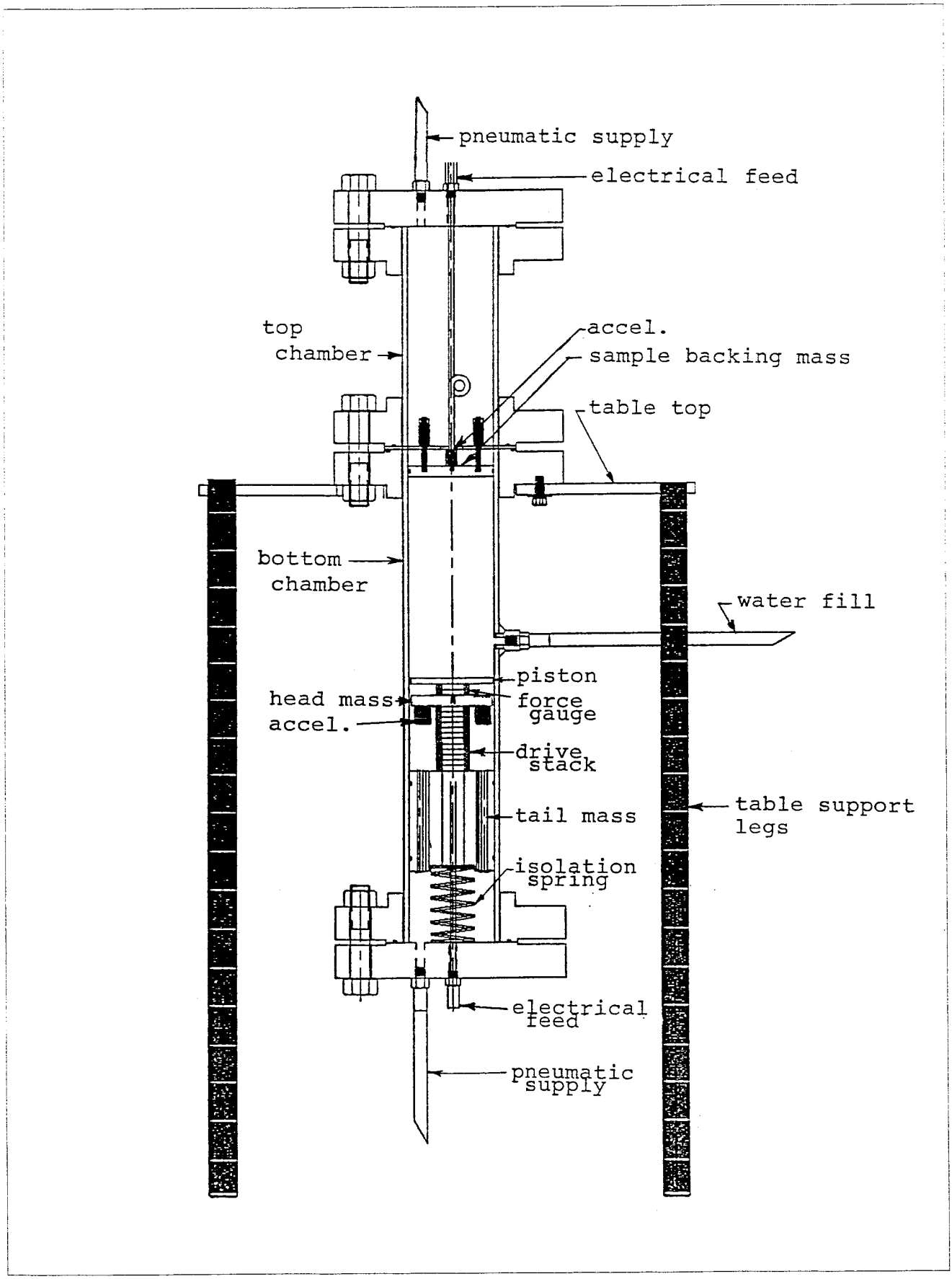

Fig. 1 - Testing device components and connections.

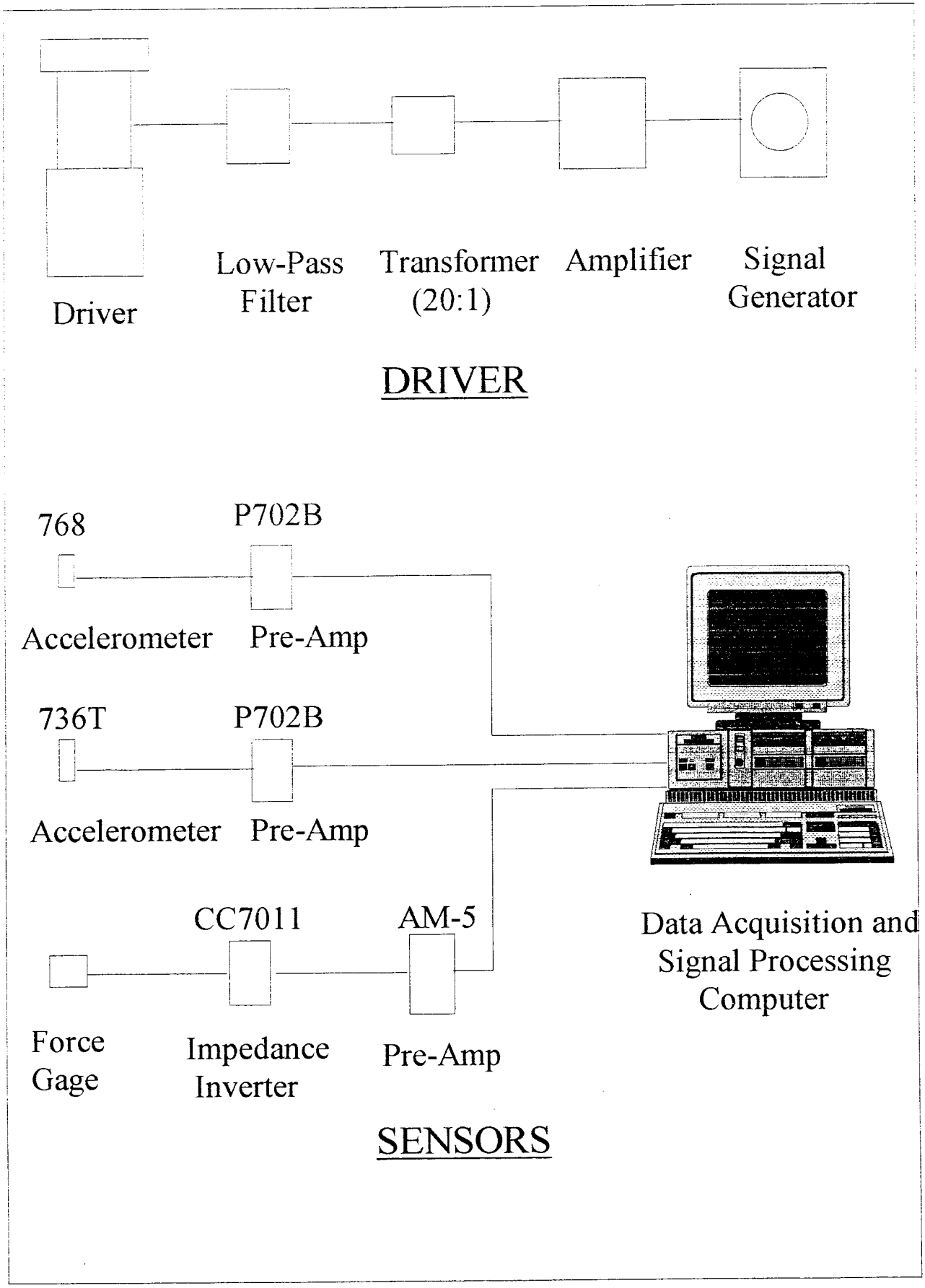

Fig. 2 - Schematic of excitation and sensor electronics.

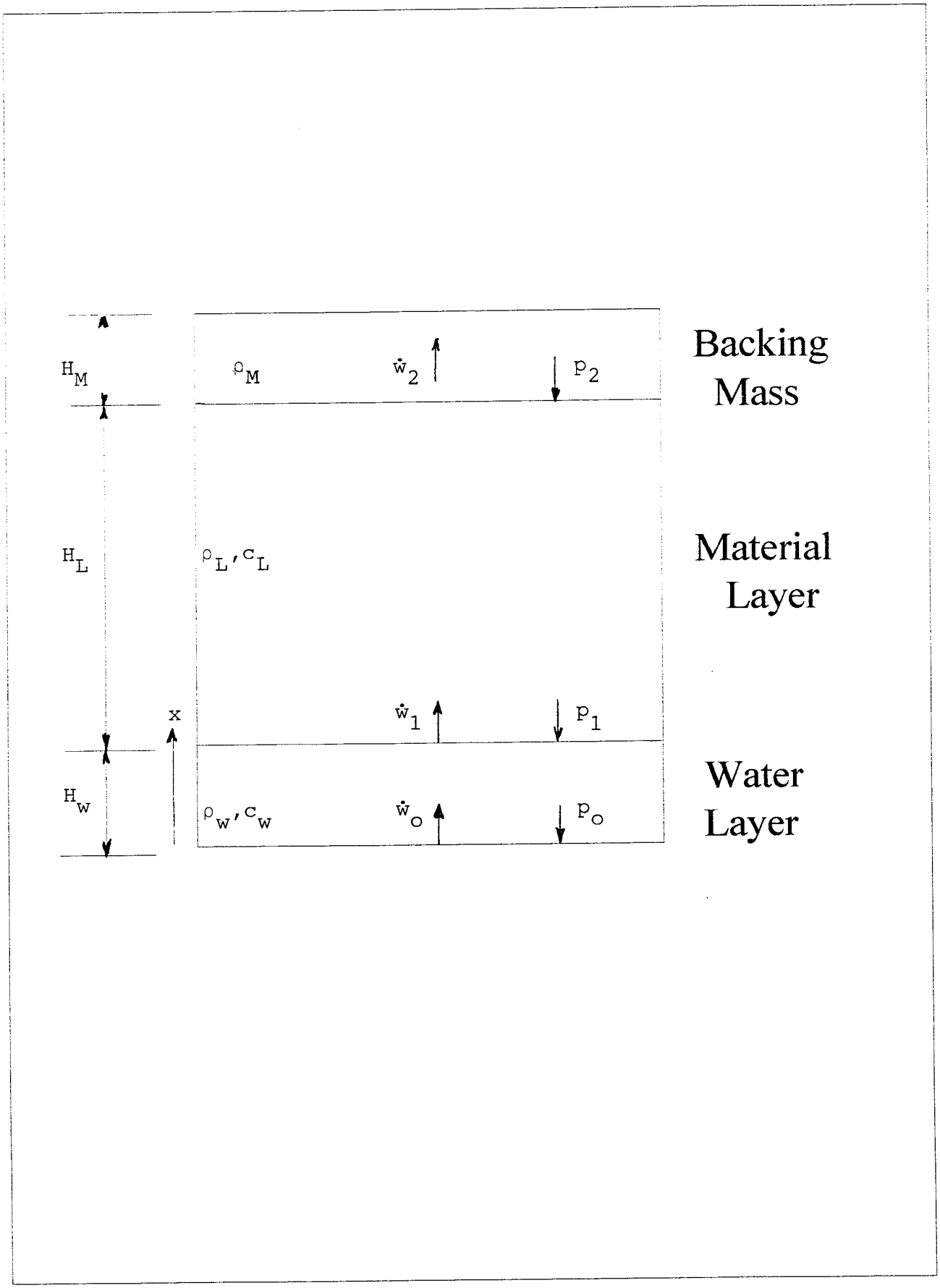

Fig. 3 - Plane wave model of material sample with water layer and backing mass.

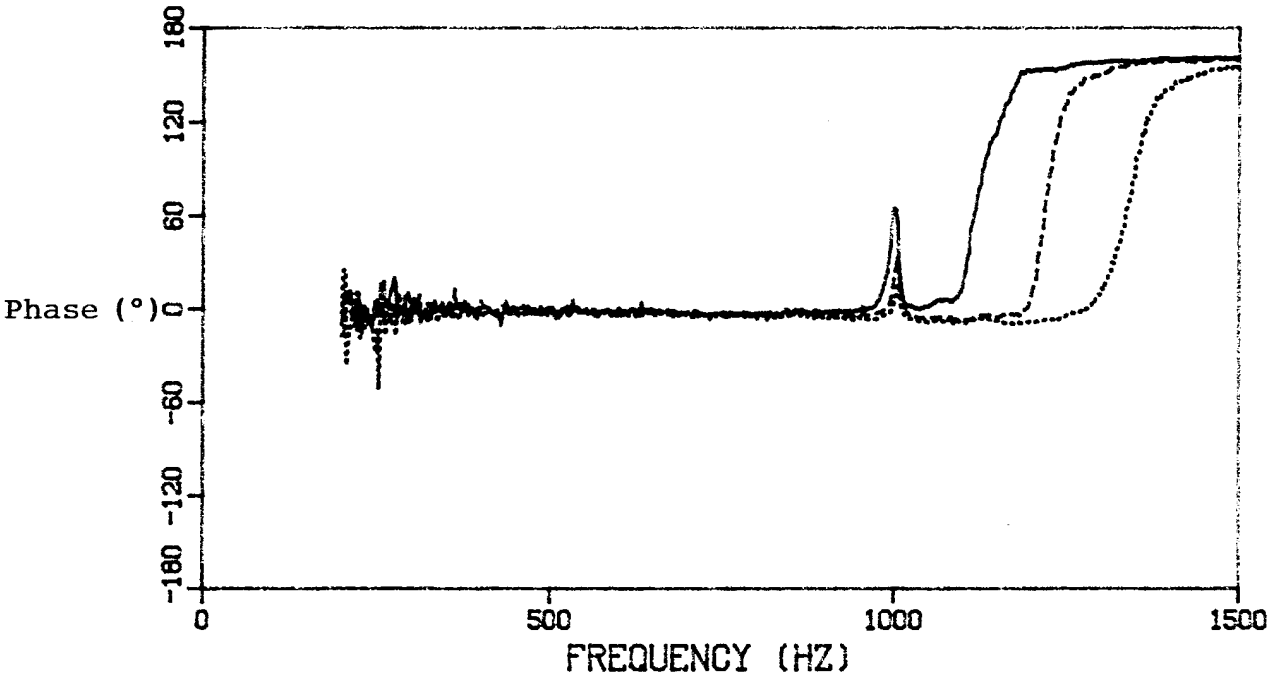

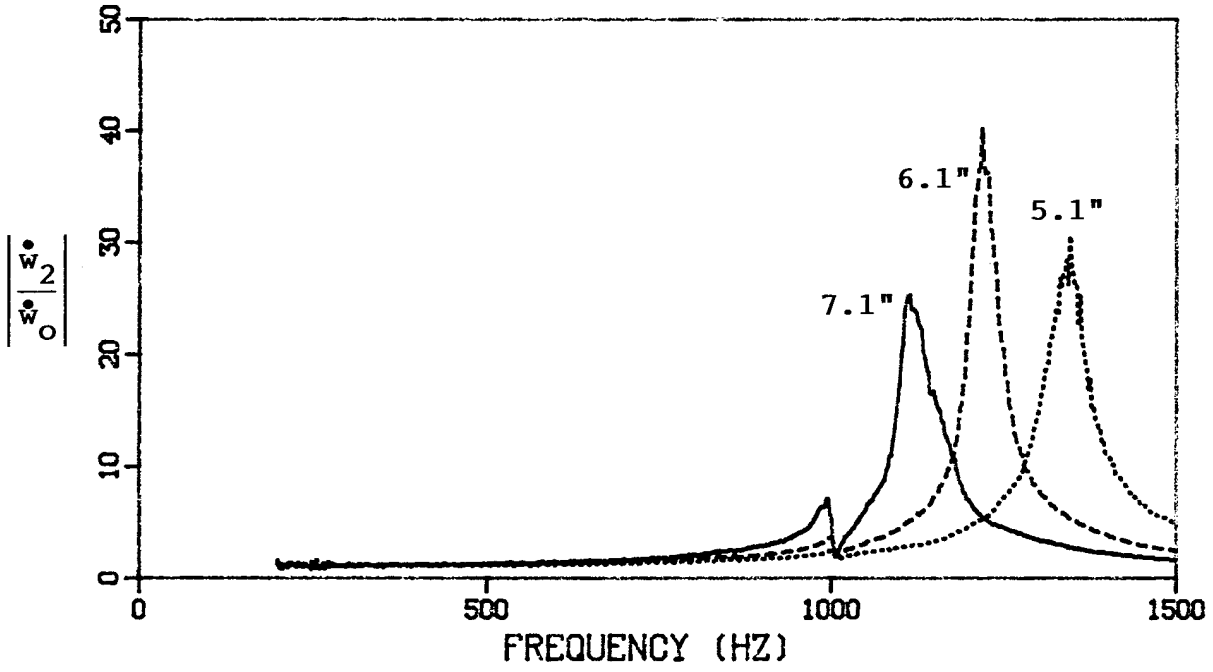

Fig. 4a - Vibration transmissibility of 5.1", 6.1" and 7.1" water columns and backing mass measured with a 2,000 Hz bandwidth chirp.

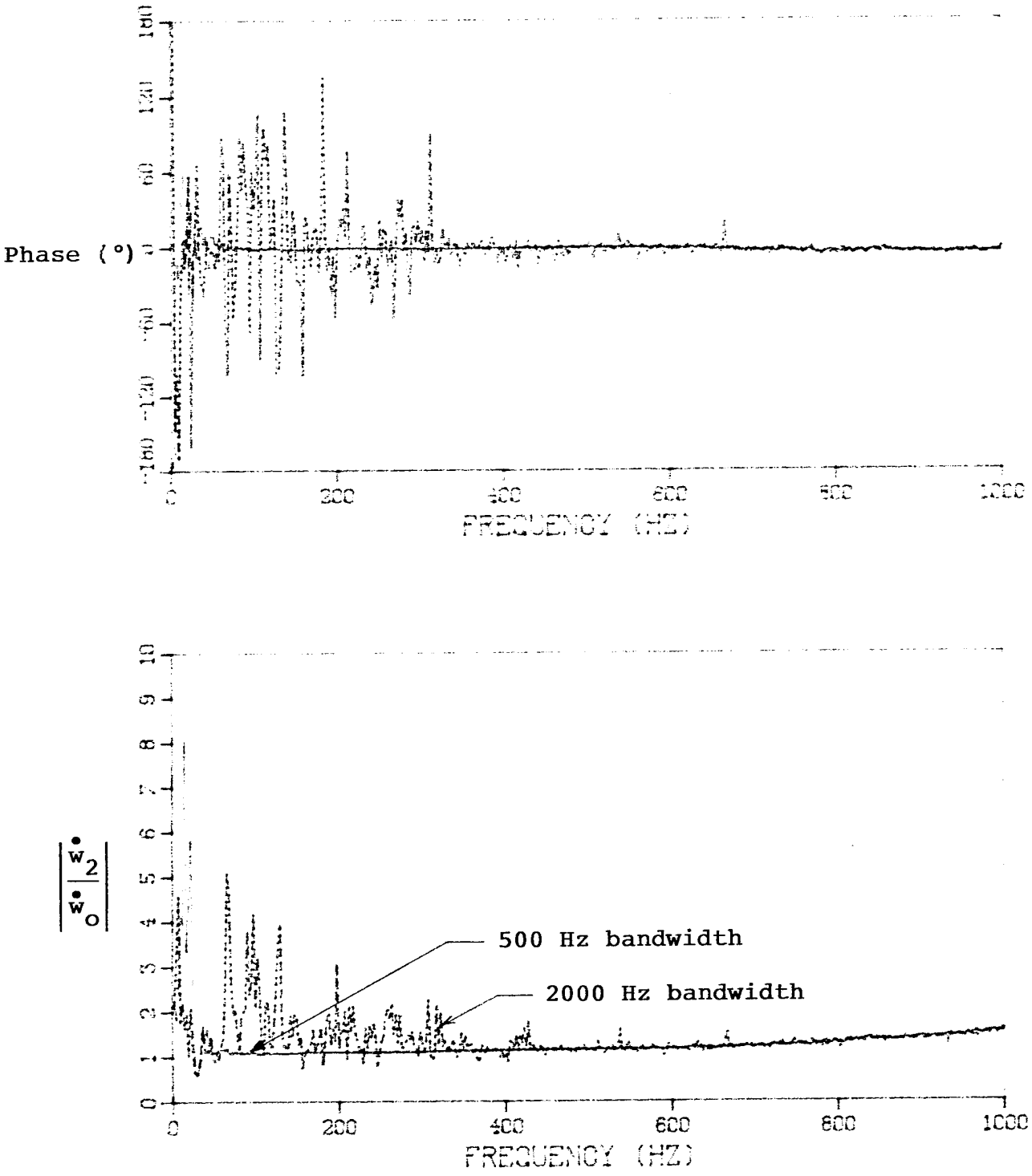

Fig. 4b - Vibration transmissibility of a 3.1" water column measured with 2,000 Hz (dash) and 500 Hz (solid) bandwidth chirps.

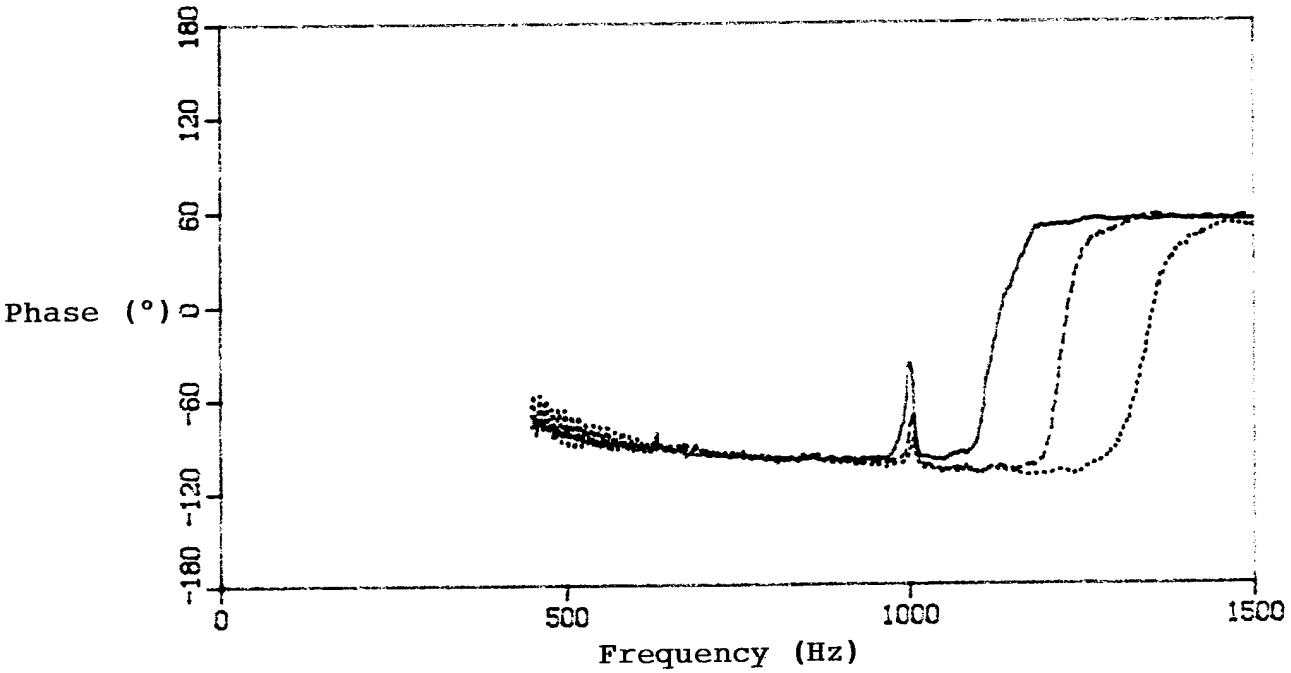

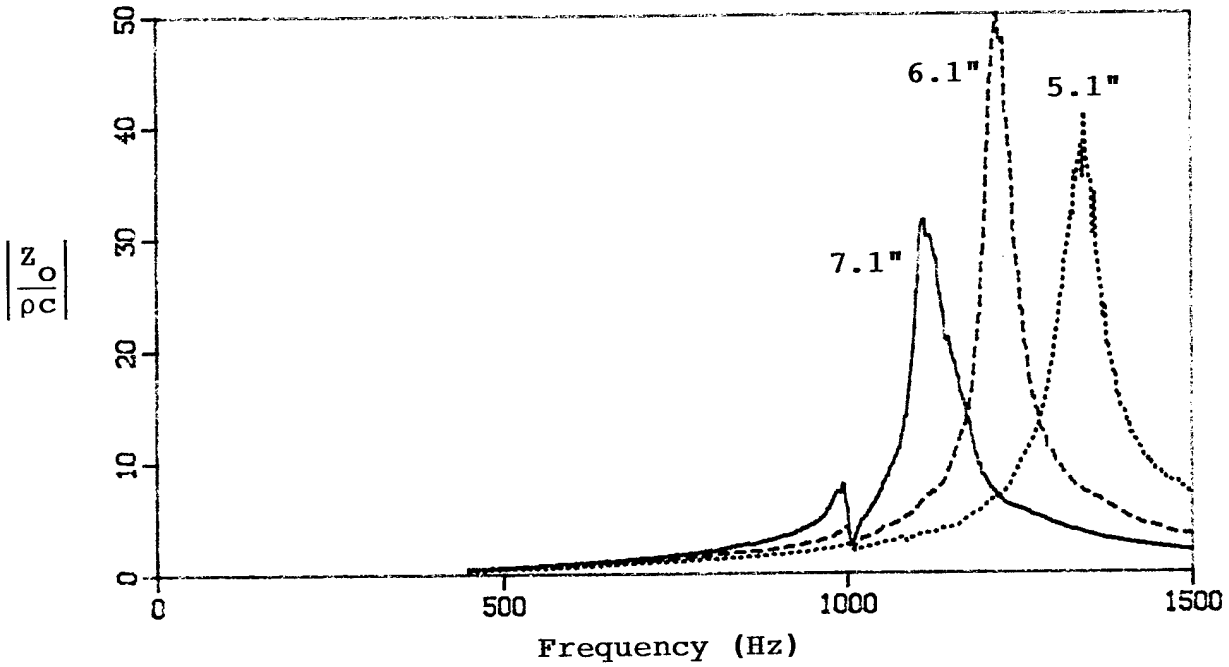

Fig. 4c Input impedance of 5.1", 6.1" and 7.1" water columns and backing mass measured with a 2,000 Hz bandwidth chirp.

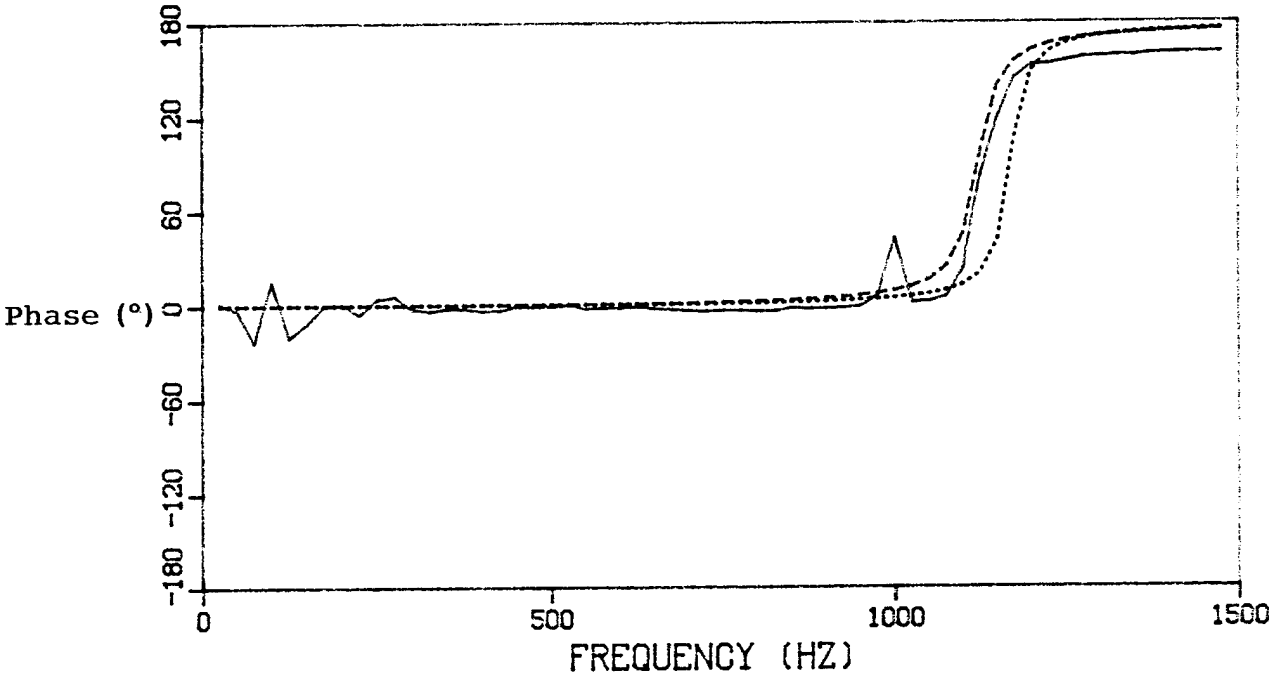

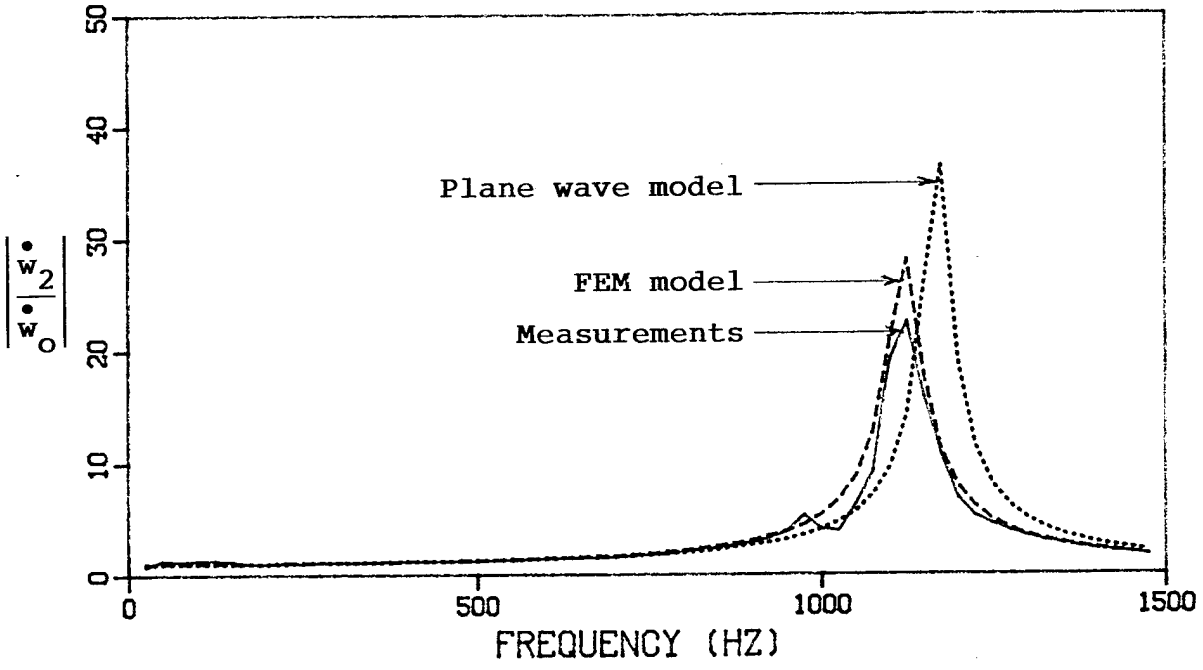

Fig. 5a - Comparison of the measured vibration transmissibility for a 7.1" water column with predictions from finite element and plane wave models.

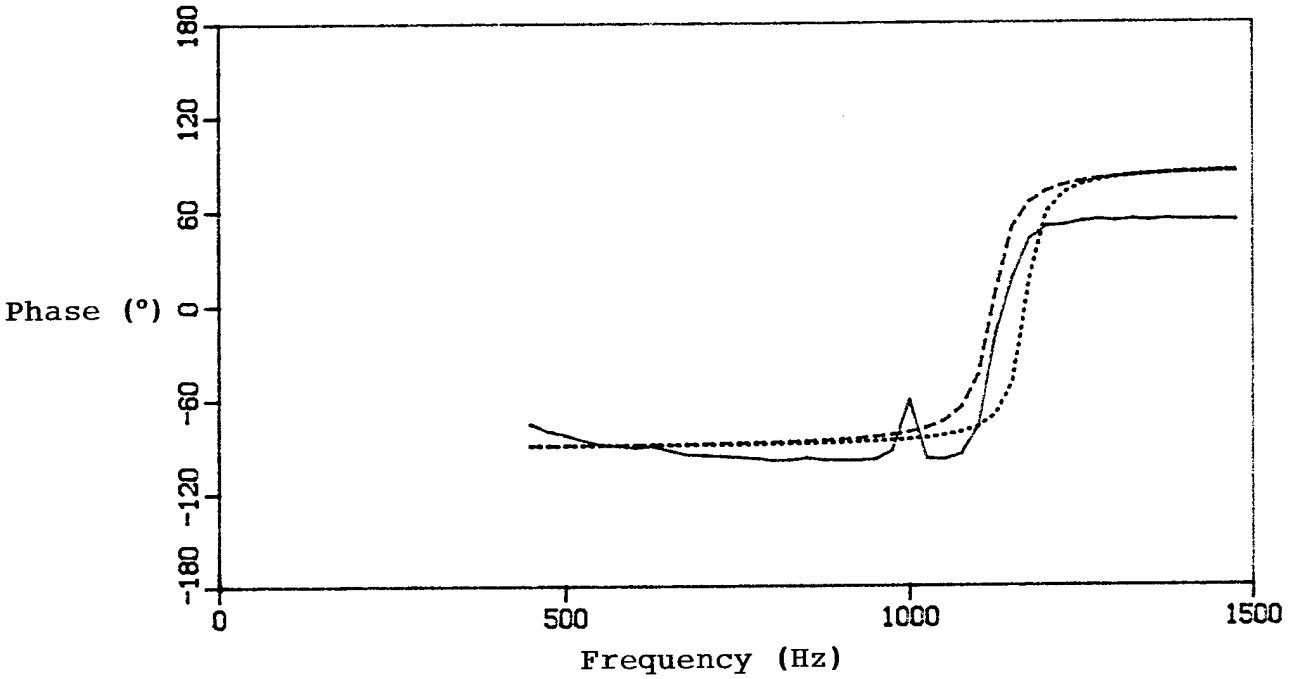

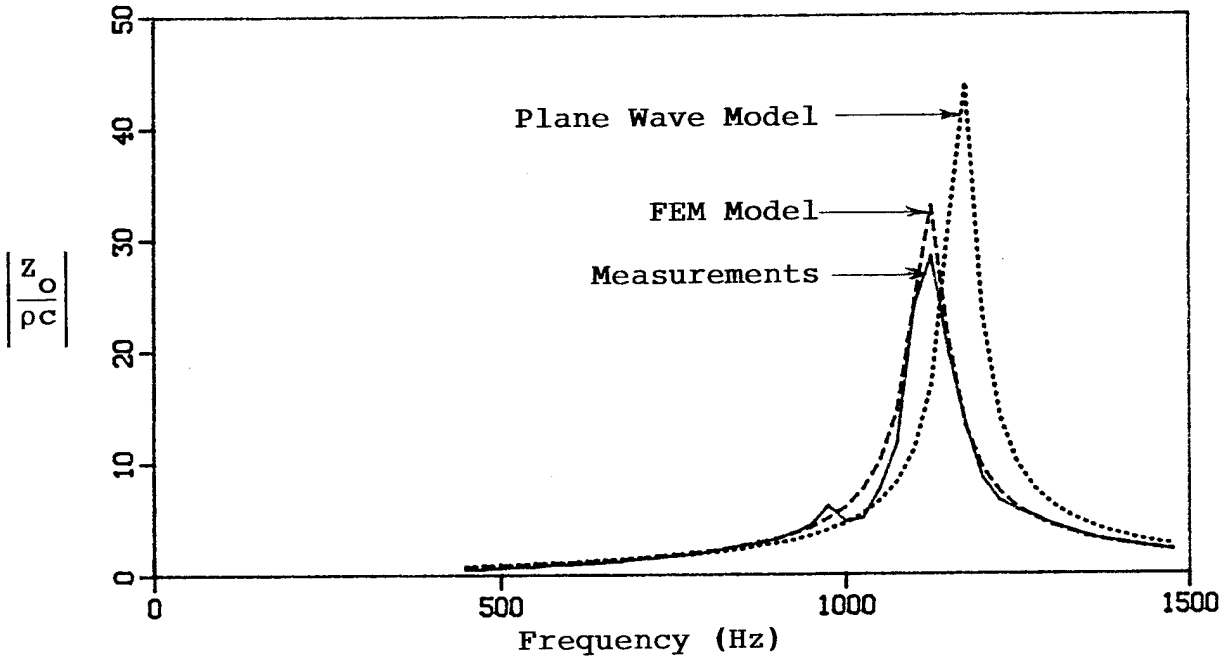

Fig. 5b - Comparison of the measured input impedance for a 7.1" water column with predictions from finite element and plane wave models.

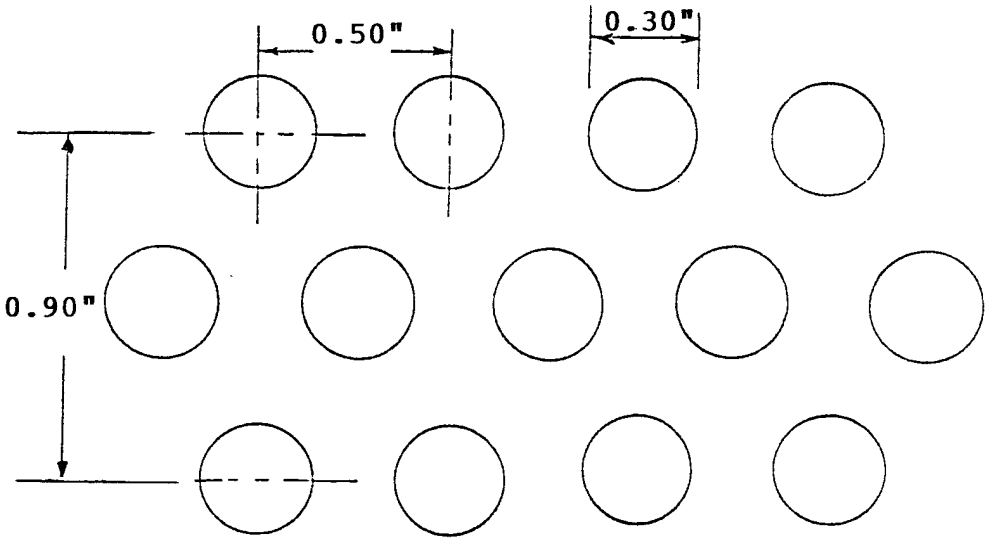

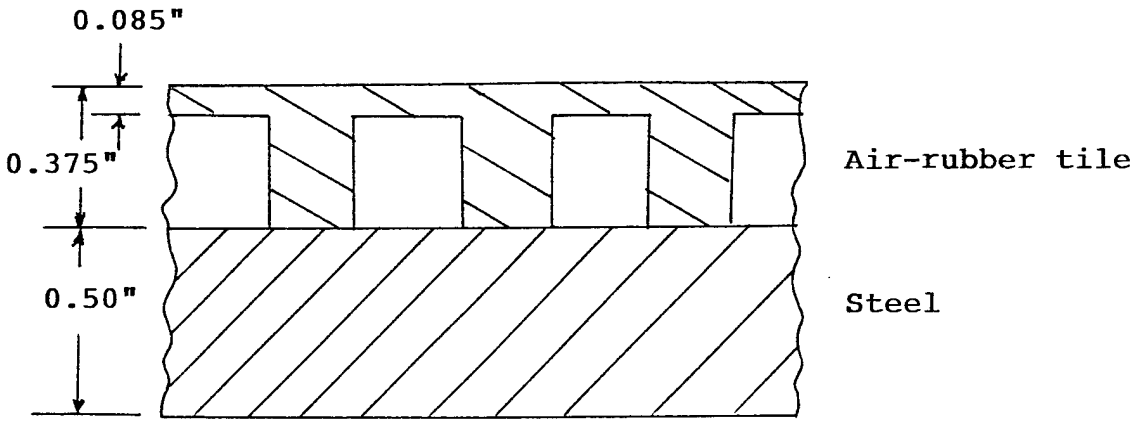

Fig. 6 - Air-rubber sample dimensions and hole pattern.

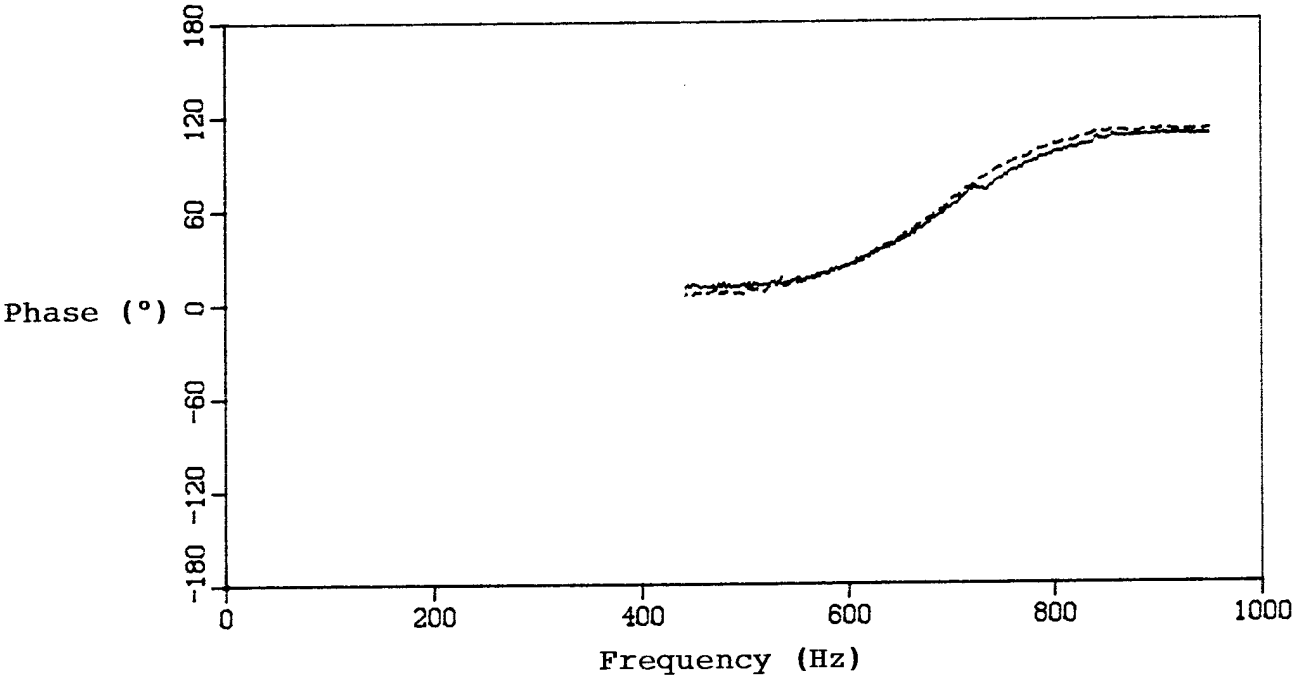

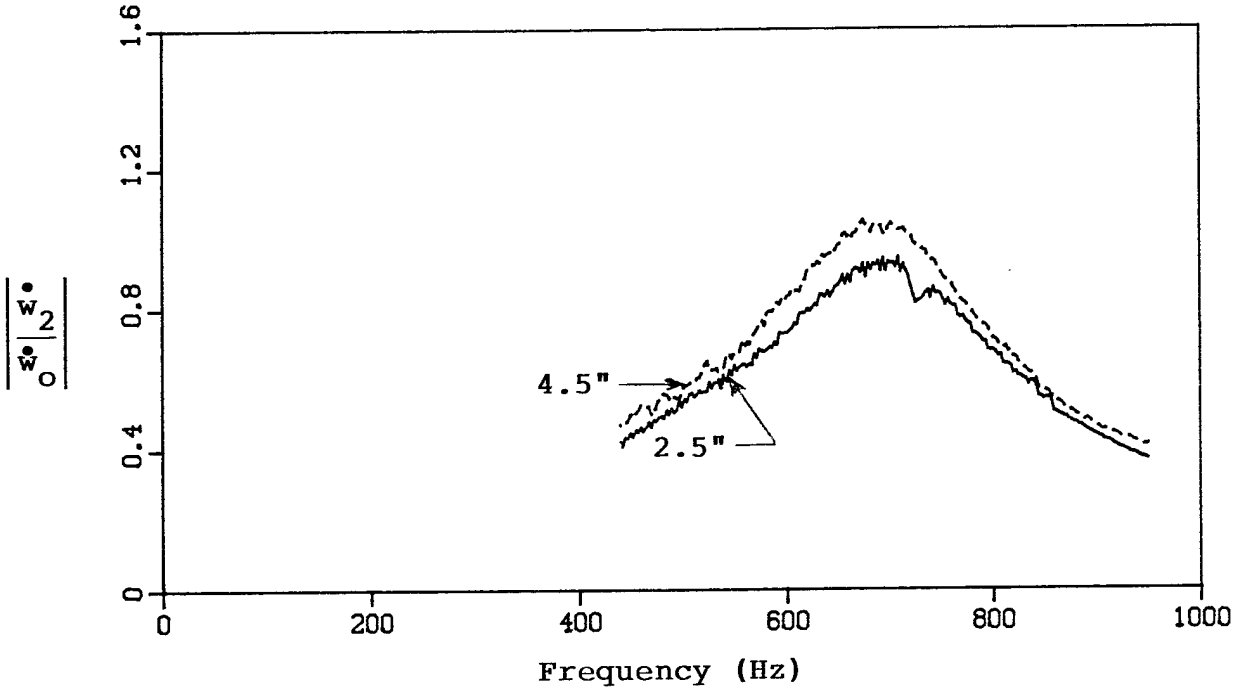

Fig. 7a Vibration transmissibility of the material sample with 2.5" and 4.5" water layers at 50 psia.

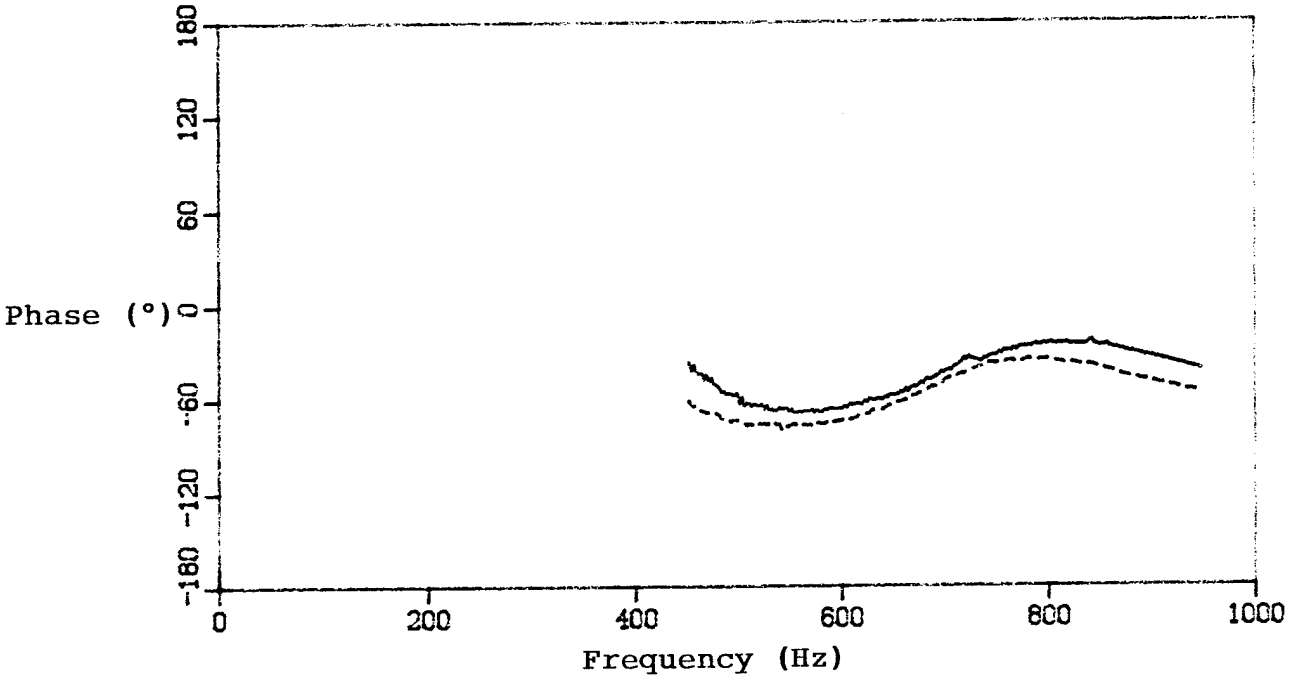

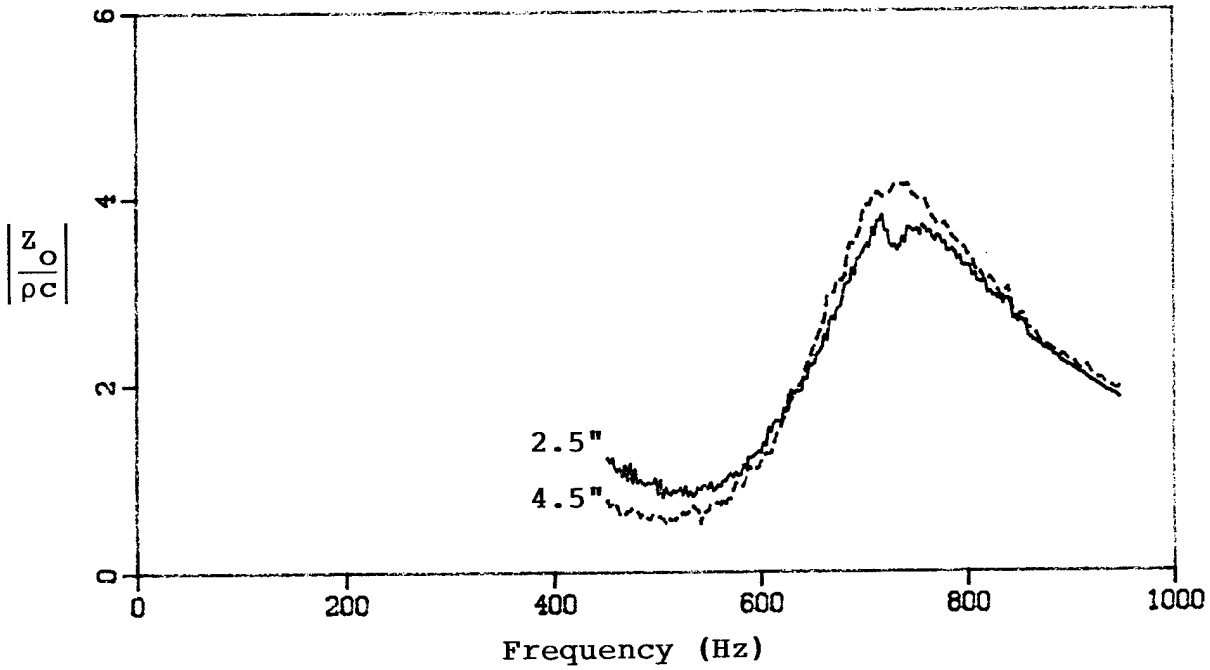

Fig. 7b Input impedance of the material sample with 2.5" and 4.5" water layers at 50 psia.

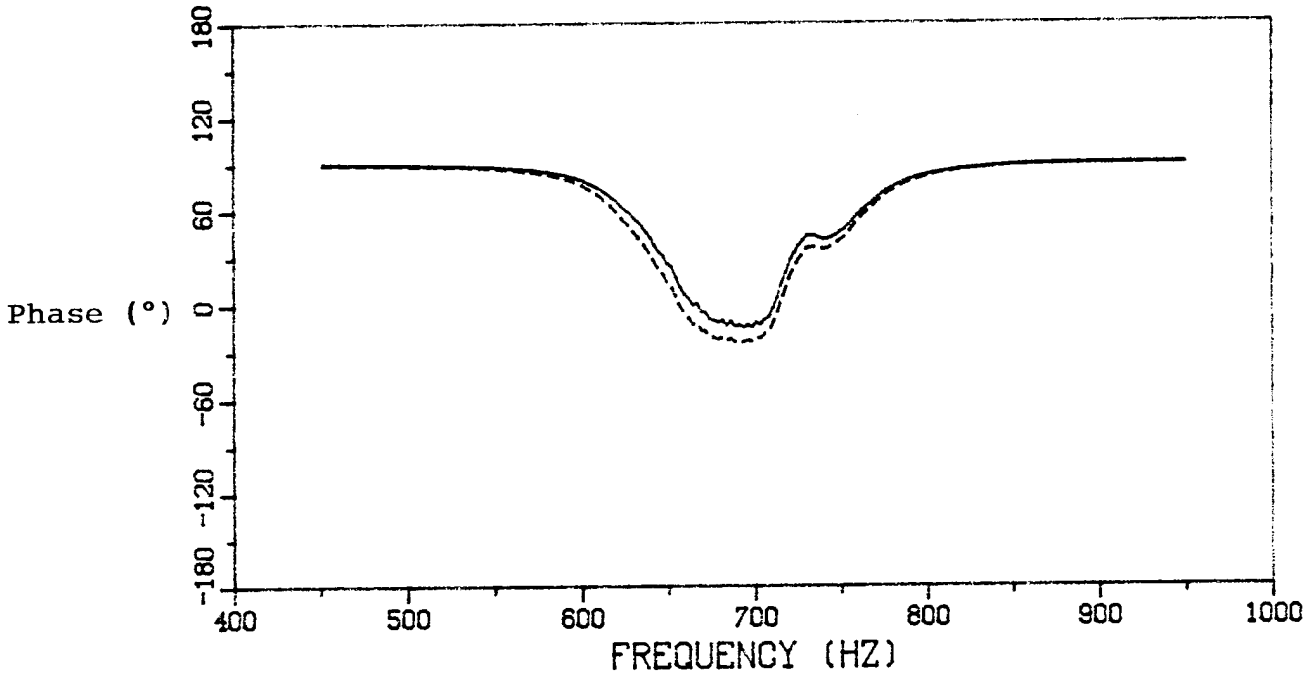

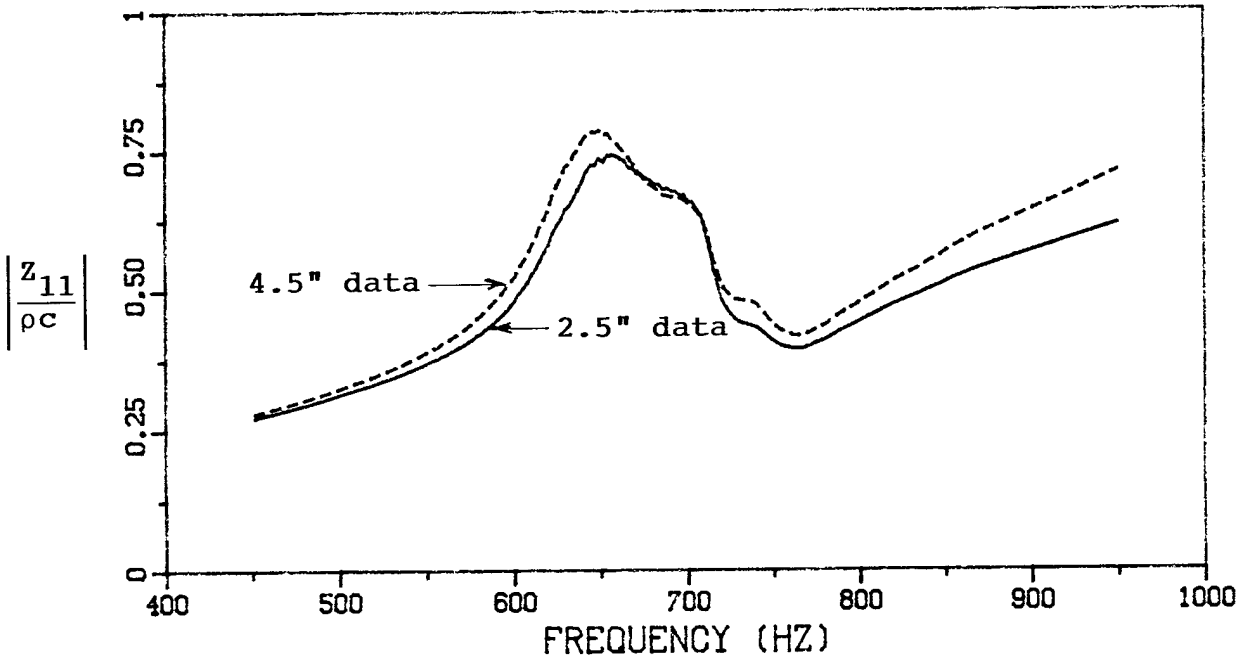

Fig. 8a - Material sample impedance Z_{11} derived from the measurements of Figs. 7a and 7b.

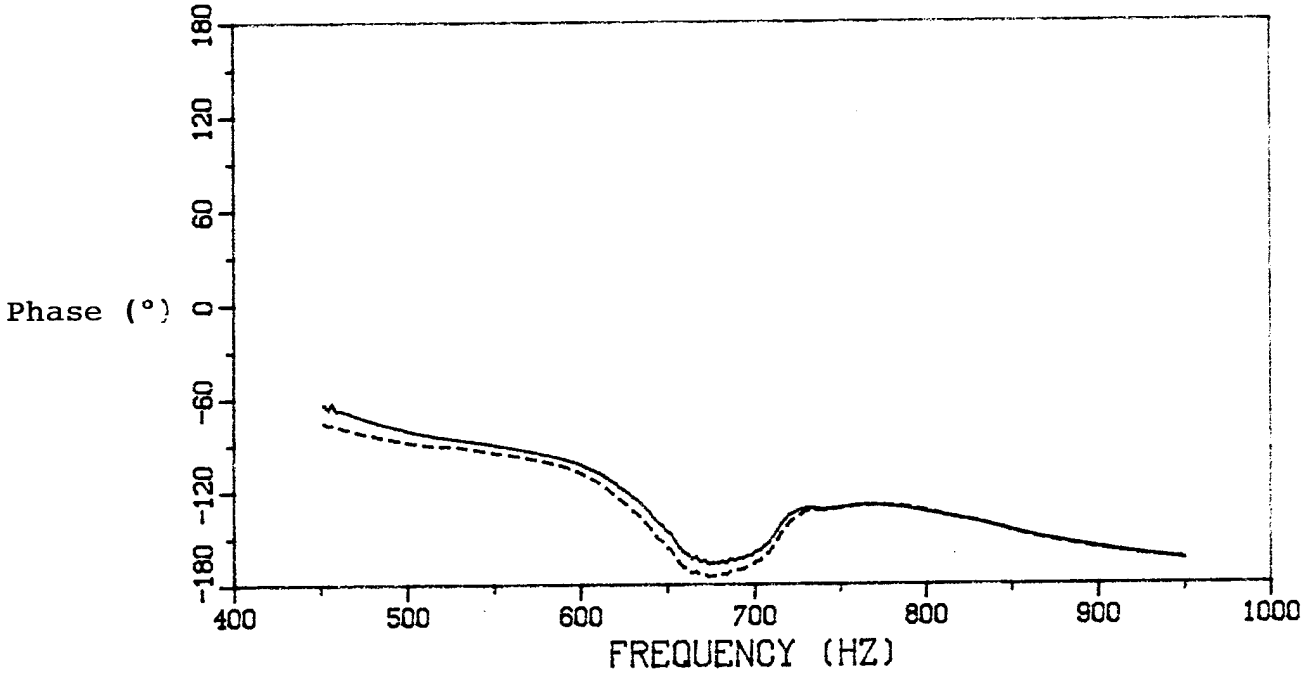

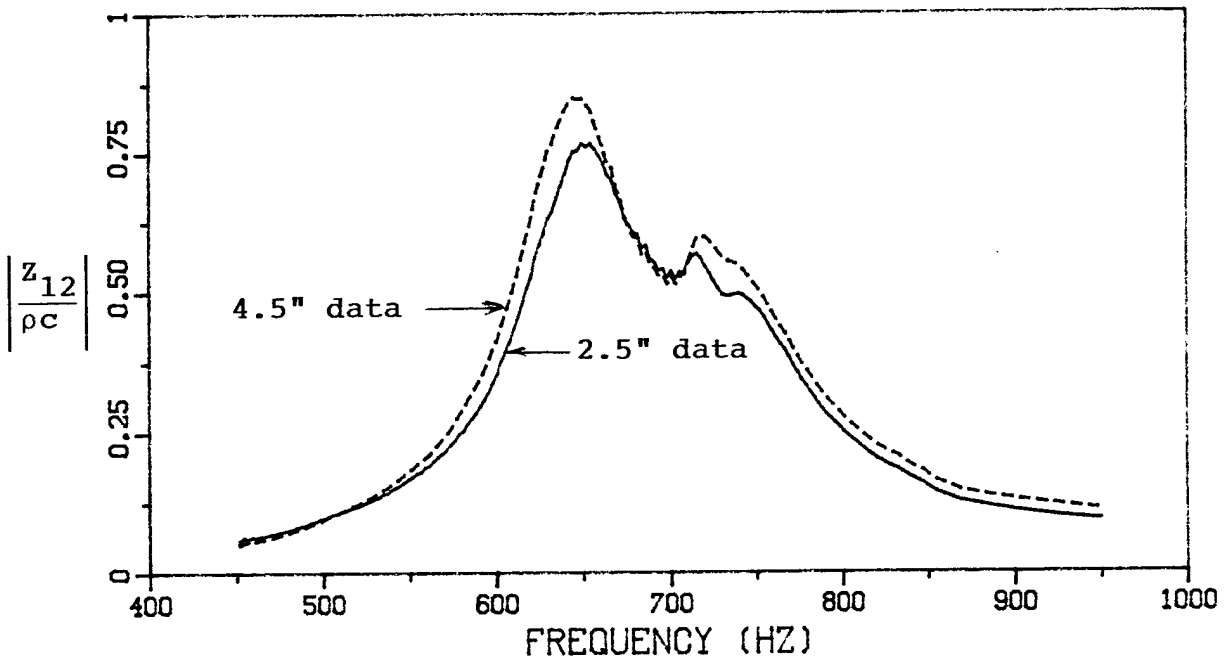

Fig. 8b - Material sample impedance Z_{12} derived from the measurements of Figs. 7a and 7b.